WPMAT-PR(17) 17958

M Klimenkov et al.

# Effect of irradiation temperature on microstructure of ferritic-martensitic ODS steel

Preprint of Paper to be submitted for publication in
Journal of Nuclear Materials

This work has been carried out within the framework of the EUROfusion Consortium and has received funding from the Euratom research and training programme 2014-2018 under grant agreement No 633053. The views and opinions expressed herein do not necessarily reflect those of the European Commission.

# Effect of irradiation temperature on microstructure of ferritic-martensitic ODS steel

M. Klimenkov*, R. Lindau, , U. Jäntsch, A. Möslang

Karlsruhe Institute of Technology, Institute for Applied Materials (IAM-AWP), Eggenstein-Leopoldshafen, Germany

*Abstract:*

The EUROFER-ODS alloy with 0.5% $Y_2O_3$ was neutron irradiated with doses up to 16.2 dpa at 250°C, 350°C and 450°C. The radiation induced changes in the microstructure (e.g. dislocation loops and voids) were investigated using transmission electron microscopy (TEM). The number density of radiation induced defects was found to be significantly lower than in EUROFER 97 irradiated at the same conditions. It was found that the appearance and extent of radiation damage strongly depend not only on the irradiation temperature but also on the local number density and size distribution of ODS particles. The higher number density of dislocation loops and voids was found in the local areas with low number density of ODS particles. The interstitial loops with Burgers vector of both 1/2<111> and <100> types were detected by imaging using different diffraction conditions.

Keywords: Ferrtitc-martensitic ODS steel; EUROFER-ODS; Neutron irradiation; Burgers vector, WBDF

Corresponding author: Michael Klimenkov
Institute for Applied Materials (IAM)
Karlsruhe Institute of Technology
Hermann-von-Helmholtz-Platz 1
76344 Eggenstein-Leopoldshafen, Germany

Phone: +49 721 608 2 2903
Fax: +49 721 608 2 4567
email: michael.klimenkov@kit.edu

## 1. **Introduction:**

Materials research for innovative nuclear fission and fusion systems has become a field of growing relevance worldwide [1]. The development of new "reduced-activation materials" that decay faster than conventional alloys by several orders of magnitude is essential for the construction of future fusion power reactors. EUROFER 97 with 9 % Cr has become the Europeans reference reduced-activation ferritic-martensitic (RAFM) steel for the fabrication of structural components for future fusion reactors. Three industrial batches of EUROFER 97 have been produced in the last 20 years in total amount of 22 tons and a broad variety of product forms relevant for the production of breeding blanket modules were manufactured. This European reference steel with composition 9Cr1WVTa has been extensively characterized under relevant conditions in the un-irradiated and irradiated state [2–5], and it's the only RAFM steel that has been qualified for the design code RCC-MRx [6]. In order to further increase the operational temperature and thus the efficiency of advanced blanket concepts for fusion reactors, an oxide-dispersion-strengthened (ODS) variant of EUROFER was developed.

Neutron irradiation and ion implantation are both experimental techniques applied for the verification of radiation resistance of ODS steels [7–11]. The advantages of ion implantation such as relatively low costs, short irradiation time and providing non-radioactive samples which allow to investigate and handle the specimens in usual preparation Labs for post implantation examination is reflected in numerous studies on ODS steels [7–9]. The latter statement depends of course on the ion energy. In high-energy ion-irradiation experiments above the activation threshold like in [12,13] the specimens undergo nuclear reactions which produce radioactive nuclides in the material. Enormous technical effort and costs for neutron irradiation experiments lead to the situation that only little published work could be found in scientific literature during the last decade [10,11]. Moreover, most of the studies were dedicated to prove the stability of ODS particles and to lesser extent to show the formation of radiation induced defects [10]. Jung et. al. have studied the defect formation in PM2000 alloy after neutron irradiation at 500°C. However, as neutron irradiated EUROFER-ODS steel shows in a wide temperature window superior tensile and fatigue properties compared to casted steels like EUROFER [14], the knowledge about the mechanisms of defect formation is important to understand the effect of ODS particles on radiation resistance and the relationship between irradiation modified microstructures and mechanical properties. Besides a detailed defect analysis, the present study also demonstrates that the formation of radiation induced defects depends not only on the irradiation temperature but also on the local distribution of ODS particles (i.e. size and local number density).

## 2. **Experimental:**

The investigated alloy EUROFER-ODS was produced on the base of the European RAFM steel of with a basic composition of about 8.9 wt% Cr, 1.1 wt% W, 0.2 wt% V, 0.14 wt% Ta, 0.42 wt% Mn, 0.06 wt% Si, 0.11 wt% C and Fe for the balance by addition of 0.5wt% $Y_2O_3$. The production process included inert gas atomisation of EUROFER (H.C. Starck) and subsequent mechanical alloying in industrial ball mills of attritor type by Plansee GmbH. Hot isostatic pressing was chosen as the appropriate consolidation process for the production of four bars of each heat 60 mm in diameter and 300 mm in length. Part of the material was made available to other European laboratories [15]. The irradiation was carried out in the Petten High Flux Reactor (HFR) in the framework of the HFR Phase IIb (SPICE) irradiation project at a nominal dose of 16.3 dpa and at three irradiation temperatures of 250°C, 350°C and 450 C, respectively [16].

The specimens for TEM investigations were prepared in the usual way by cutting, grinding, and electrochemical etching. Disks with a thickness of 0.2 to 0.3 mm and 3 mm in diameter were thinned by electropolishing in a TENUPOL V device using $H_2SO_4$ + 80 % $CH_3OH$ electrolyte. In the next step disks of 1 mm in diameter with the hole in the middle were punched in order to minimize the mass of the radioactive sample and thus the irradiation exposition and optical distortion by the magnetic field. TEM investigations were performed using a FEI Tecnai 20 FEG analytical microscope with an accelerating voltage of 200 kV. All the preparation and analytical work on the irradiated samples was done in the controlled area of the Fusion Materials Lab at KIT.

The determination of Burgers vector of dislocation loops has been performed by weak beam dark field (WBDF) imaging with low indexed $\boldsymbol{g}$(n$\boldsymbol{g}$) vectors near [100] and [111] zone axes. The tilting experiments were performed using standard FEI double tilt holder. The corresponding visibility criteria of dislocation loops for different $\boldsymbol{g}$ vectors are described in tables 1 and 2.

## 3. **Results:**

### 3.1 Microstructure of unirradiated material

The grains in EUROFER-ODS alloy with 0.5% $Y_2O_3$ have mainly a size of several microns (Fig. 1). The material shows a ferrite grain structure since formation of martensite laths inside grains was not detected. The analytical 2D investigations show the presence of two types of precipitates: $M_{23}C_6$ carbides, where M = Cr, Fe, W, Ta, V (Fig. 1b) and fine dispersed $Y_2O_3$ particles (Fig. 1c). The spatial distribution of $M_{23}C_6$ phase is well visible in the Cr elemental map (Fig. 1b). $M_{23}C_6$ precipitates with elongated shape are often located on grain boundaries, however, rarely they could be found inside grains. The depletion of Cr in the vicinity of grain boundaries was clearly detected (Fig. 1b). This effect is presumably caused by preferential Cr diffusion along grain boundaries toward $M_{23}C_6$ carbides. In general, the grain structure and distribution of ODS particles are very similar to that of EUROFER-ODS alloy with 0.3% $Y_2O_3$. Its detailed microstructural characterization was published in the past [17,18].

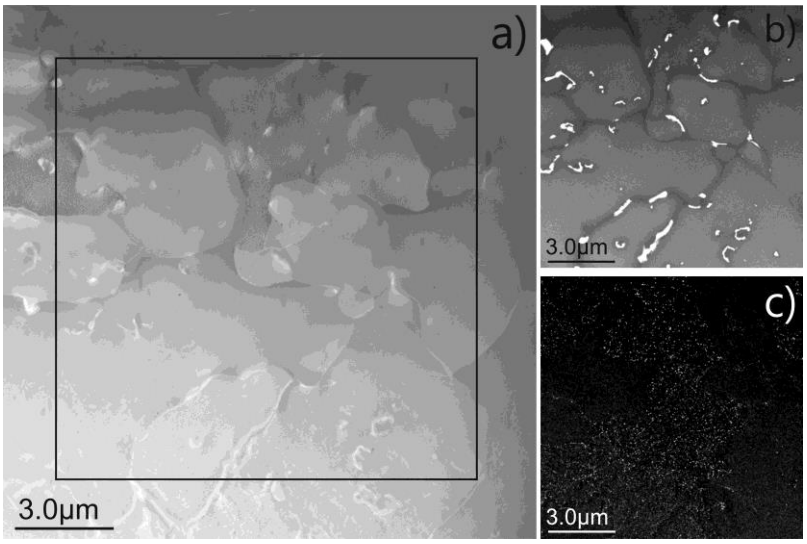


Fig. 1. Microstructure of unirradiated EUROFER-ODS material. The HAADF image is shown in part (a), Fe and Cr maps demonstrating the distribution of $M_{23}C_6$ precipitates are presented in the parts (b), and (c), respectively.

Analytical investigations demonstrating the distribution of ODS particles are shown in Fig. 1c and Fig. 2. The HAADF image of investigated area is given in Fig. 2a, while the Y-L EDX elemental maps of the marked areas (dashed black and white rectangles) are presented in the parts (b) and (c) respectively. These both elemental maps were obtained from different scan experiments: in the part (b) the raw scan was performed with 15nm step size, whereas elemental map shown in part (c) was obtained with the scan step and probe size of about 2 nm. The second scan allows detection of even small ODS particles with few nanometer size.

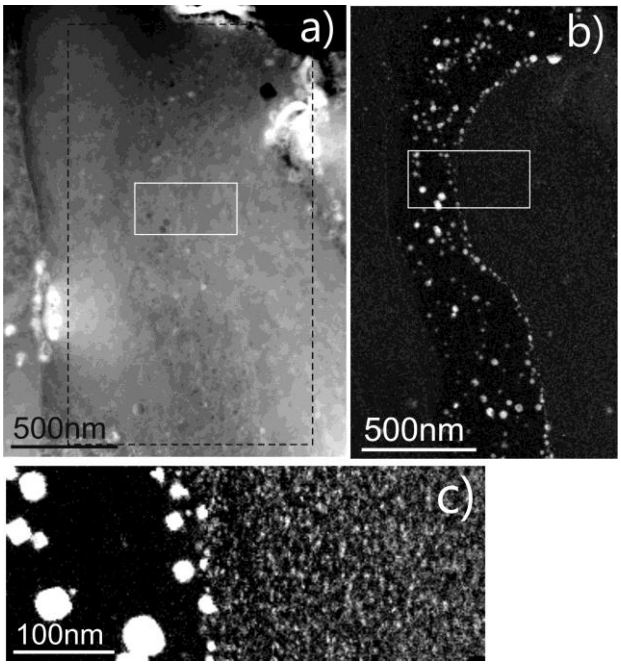


Fig. 2. The elemental maps demonstrate the distribution of ODS particles. The HAADF image of the investigated area is shown in part (a). The Y map of the marked area is shown in part (b), and also in the marked small rectangular obtained with a scanning step of 1.5nm is shown in part (c).

The results demonstrate that $Y_2O_3$ ODS particles have a bimodal size distribution. This means that two areas with completely different spatial distribution and morphology of ODS particles exist. The "coarse area" is the region, where the size of ODS particles varied from 5 nm to 18 nm with a number density of $(2\pm0.5)*10^{20}m^{-3}$ (Fig. 2b middle, Fig. 2c left side). The "fine area" shows a very homogenous distribution of ODS particles with sizes less than 5 nm. The number density in the fine area was measured to $(1.0\pm0.3)*10^{22}$ $m^{-3}$ (~70 times higher than in the "coarse area"). Contrary to the "coarse area" only few ODS particles with sizes larger than 5nm were found in the "fine area".

The ODS particles in the "fine area" are hardly visible in the TEM images. The application of bright field TEM or HAADF imaging does not deliver satisfying imaging results. The high resolution TEM investigations suggest that these nano-sized particles do not show any defined crystalline structure and possibly they do not have a stoichiometry of $Y_2O_3$. Such small ODS nanoparticles are often referred to as nanoclusters [19]. Our experience show that the nano-particles are well visible only in two-dimensional elemental Y-L maps obtained with ~2 nm (or better) spot resolution. The existence of areas with different distribution of ODS particles, known as "bimodal distribution", was already discovered in a previous works [20]. Often a bimodal distribution is accompanied by changes in the grain sizes. As it is shown in ref. [21] the "coarse area" is normally located in the region with grains smaller than 70 nm whereas the formation of nanoclusters or "fine areas" was observed in the large grains of 2-3 µm size. In our material the distribution of ODS particles and nanoclusters in coarse and fine areas does not correlate with the grain structure (Fig. 1c, Fig.2b,c). The coarse area can be located inside grains surrounded by fine area or vice versa. Due to the significantly different formation of

radiation induced defects hereinafter the two these different areas will be referred to as "**coarse area**" and "**fine area**".

### 3.2 **Investigation of irradiated materials**

Two types of radiation induced defects – cavities and dislocation loops were observed and extensively characterized by TEM. Quantitative analysis of dislocation loops, that means determination of Burgers vector and nature, i.e. interstitial or vacancy loop, was performed by imaging of some selected grains with **g**-vectors of <011> and <002> types in orientation close to the [100] or [111] zone axes. The visibility criteria (|g·b| values) for each ***g*** vector near the mentioned zone axes are listed in tables 1 and 2. study of irradiated materials.

#### *3.2.1 Investigation of specimen irradiated at 250°C*

Fig. 3 represents the investigation of structural defects and identifying their Burgers vectors in material irradiated at 250°C. The grain was selected in such a way that imaging of "coarse" and "fine areas" can be done in the same micrograph. The "fine area" with only few dislocations is located in the upper part of the micrograph. The "coarse area", which shows a 10-15 times higher density of dislocations, is located in the bottom parts of micrograph. The four WBDF micrographs imaged with reverse contrast were obtained with 4 different ***g*** vectors (i.e. **g**(2**g**) [011], **g**(3**g**) [$01\bar{1}$], **g**(2**g**) [020] and **g**(2**g**) [002]) close to the [100] zone axis. The diffraction vectors used to excite the dislocations are drawn in the micrograph.

The analysis shows that all dislocations present in the investigated area are visible in both **g**(2**g**) images with ***g***=[020] and **g**(2**g**) with ***g***=[002] (Fig. 3c,d). These dislocations are also visible either in a (**g**3**g**) image with ***g***=[011] (part a) or in **g**(2**g**) image with ***g***=[$01\bar{1}$] (part b). It can be concluded that all line dislocations in this area have Burgers vector of ***b***=½<111> type. Moreover the Burgers vectors of 95% of all dislocations in this grain show the same projection in (100) plane: ***b***=½[$1\bar{1}1$]/½[$\overline{11}1$]. Only 3 dislocations which are visible in the image with ***g***=[011] (Fig.3a) have a ***b***=½[$\bar{1}11$]/½[111] Burgers vector. By comparing the values of dislocation densities it can be concluded that the pinning effect of line dislocations is stronger in the "coarse" than in the "fine area". All imaged dislocations are screw-type or mixed-type. The dislocations of pure screw type are visible as long straight lines (Fig. 3b-d).

These investigations demonstrate that number density of radiation induced defects is notably low. It is even difficult to surely identify them because the "dark dots" show a certain similarity

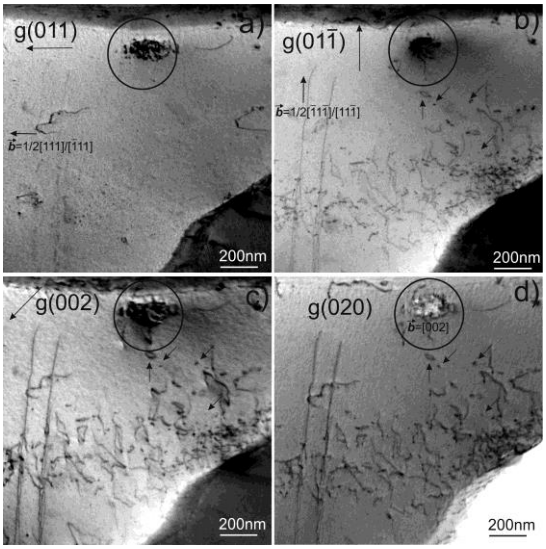


Fig. 3. Four images of specimen irradiated at 250°C obtained near [100] zone axis. The corresponding g-vectors and pronounced details are marked in the images. See text for detailed information.

to the large ODS particles. It is necessary to check visibility of the defects in all **g**-images. In most cases these defects were observed in the "coarse area" and only few individual radiation defects in the "fine area". Three dots and a dislocation loop are exemplarily marked with arrows in the [01$\bar{1}$], [020] and [002] images (Fig. 3b-d). The visibility criteria (Tab. 1) show that all these defects have the same Burgers vector like most of the dislocations, that means ½[1$\bar{1}$1]/½[ $\bar{1}\bar{1}$1]. The number density of these defects for the "coarse" area was measured to (7±3)*$10^{20}$$m^{-3}$. This value is approximately one order of magnitude lower than the number density of defects measured for EUROFER 97 irradiated at the same conditions (16dpa, 250°C) [22].

20-100nm large areas with high defect concentration were observed additionally to the described defects in the "coarse" and fine "areas". Such an area is marked with a circle in Fig. 3. Because these areas were not observed in un-irradiated material, it can be suggested that the neutron irradiation is the reason for their formation. The defects inside this area cannot be clearly differentiated from each other however it can be assumed that inside areas numerous small dislocation loops were formed. Contrary to all other dislocation lines the defects in this area show a ***b***=[001] Burgers vector. They are visible with dark contrast in ***g***=[011], ***g***=[01$\bar{1}$] and in ***g***=[020] images invisible or rather have a bright contrast in the ***g***=[002] image.

.

| ***g*** \ ***b*** | ½[111] | ½[$\bar{1}$11] | ½[1$\bar{1}$1] | ½[11$\bar{1}$] | [001] | [010] | [100] |
|---|---|---|---|---|---|---|---|
| [011] | 1 | 1 | 0 | 0 | 1 | 1 | 0 |
| [01$\bar{1}$] | 0 | 0 | 1 | 1 | 1 | 1 | 0 |
| [002] | 1 | 1 | 1 | 1 | 2 | 0 | 0 |
| [020] | 1 | 1 | 1 | 1 | 0 | 2 | 0 |

Table. 1 |b·g| values for all **g** vectors in orientations close to the [100] zone axis.

### *3.2.2 350°C specimen*

ODS material irradiated at 350°C shows a complex structure of radiation induced defects which includes dislocation loops and voids located on ODS particles. In Fig. 4 two images are presented WBDF images with **g**(3**g**) with $\boldsymbol{g}=[01\bar{1}]$ and **g**(3**g**) with $\boldsymbol{g}=[020]$ vectors obtained at

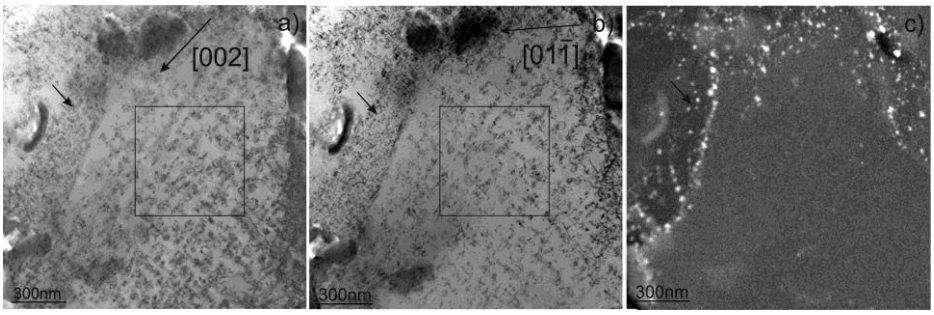


Fig. 4. The images demonstrate the distribution of dislocation loops using [002] g vector in part (a) and [01-1] g vector in part (b) in the specimen irradiated at 350°C. The distribution of ODS particles is shown in the Y elemental map (part c)

the orientation closely to the [100] zone axis (a, b) and EDX Y-K map of this area, which demonstrates the distribution of ODS particles. The "coarse" areas are quite visible at the left, upper and upper right edges of the image. These "coarse" areas (marked by a small arrow) are characterized by a 3 times higher density of dislocation loops (Fig. 4 a, b) than in the fine area which is located in the middle of the micrograph. The "fine" area marked with squares in both ***g*** images (a,b) were investigated in detail by imaging with all four ***g*** vectors near <100> zone axis ( Fig. 5a - d).

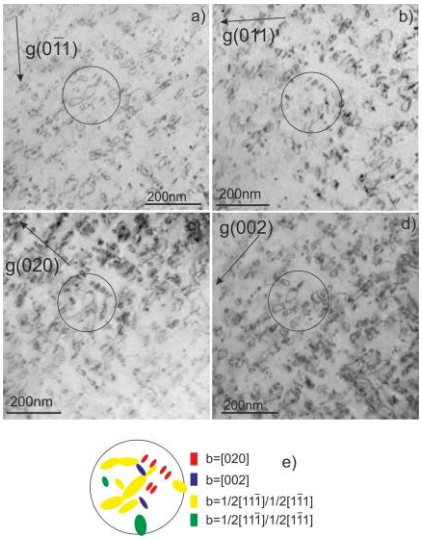


Fig. 5. The four images of the area marked with a square in Fig. 4 were obtained near [100] zone axis. The corresponding g-vectors are marked in the images. Part (e) shows the dislocation loops drawn with colors depend on the Burgers vector from the circled area in parts (a-d).

In part (e) the results of the Burgers vector analysis of dislocation loops in the circled area are shown. The different loops are imaged with different colors according to their Burgers vector; 8 loops of ½<111> type (yellow, green) and 9 loops of <100> type (red, blue) were detected. As it can be recognized in Fig. 5 inside the circle that 6 loops of <100> type (red) are ordered along crystallographic [100] direction. The Burgers vector of 5 loops in this area could not be unambiguously identified. Statistical analysis shows that the $n_{[100]}/n_{[111]}$ ratio of number densities in the fine area was measured to be 45%/55% (±15%) and 60%/40% (±15%) in the coarse area. The total number density of dislocation loops was measured to $(4\pm1)*10^{21}m^{-3}$ in the fine area and $(7\pm1.5)*10^{21}m^{-3}$ in

the coarse area. The fact that in the [100], [010] or [001] ***g*** images ½<111> loops and 1/3 of <100> loops are visible was taken into account for the calculation of the number density.

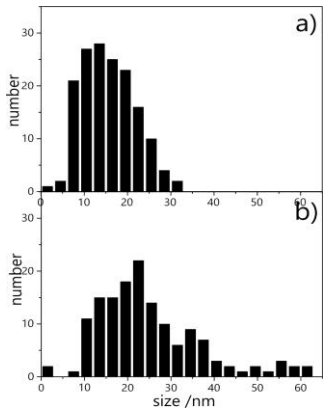


Fig. 6. Histograms showing the size distribution of dislocation loops of [100] type (a) and ½[111] part b.

The size distribution histograms of dislocation loops of both types are shown in Fig. 6. The size of <100> loops varied from 5 to 30nm with an average at 15nm (Fig. 6a), while the size histogram of ½<111> loops (Fig. 6b) shows a broad size distribution in the range from 5nm to 60nm with an average size of 26 nm. It can be clearly seen that about 25% fraction of ½<111> loops have a size larger than 30nm. It was found that in some cases <100> loops are ordered along <100> crystallographic directions.

Additional investigations were performed to determine whether the loops are of vacancy or interstitial type. The ***g*** and ***–g*** weak beam images of dislocation loops show that all loops have the same inside-outside contrast (Fig. 7). All loops in part (a) show an outside contrast, and inside contrast in part (b). Several pronounced loops are marked exemplarily with arrows in both images. The determination of the habit plane of these loops by tilting experiments allows to make the conclusion that all loops of ½<111> type have the same (1-11) habit plane and herewith they all have interstitial character.

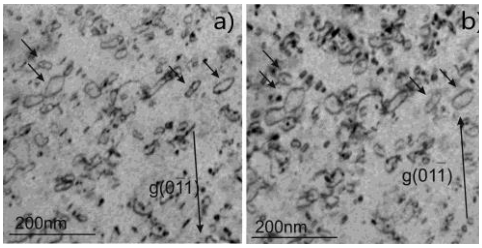


Fig. 7. g –g analysis which demonstrate that dislocation loops have interstitial character in the specimen irradiated at 350°C.

A second type of neutron radiation induced defects, namely voids were observed exclusively in "coarse area" on ODS particles. In Fig. 8 a bright field TEM image of "coarse area" with voids is shown. The coarse ODS particles itself were found in amorphous state after irradiation at all temperatures (Fig. 8b is shown here as example). The bright field image was obtained from grains oriented far from the two beam diffraction conditions in order to minimize contrast effects from the dislocation loops. The image in the part (a) where the "coarse area" is located in the center was obtained using 4.5µm defocus which

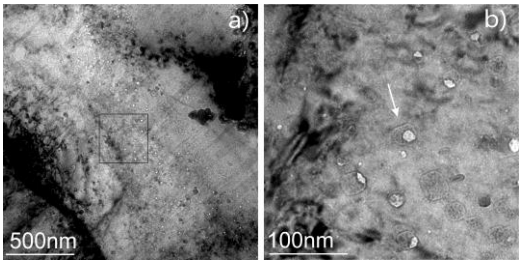


Fig. 8. Bright field images after 350° C neutron irradiation of a coarse area obtained with 1.83µm underfocus (a) and the TEM image of the marked area obtained with higher magnification.

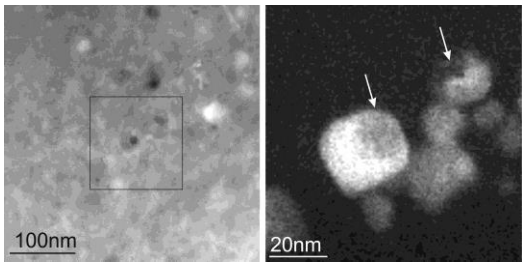


Fig. 9. Analytical investigation after 350° C neutron irradiation of ODS particles in the area marked with a square in HAADF image (a). Y map of this square is shown in the part (b).

enhances the contrast of voids. The voids are visible as numerous bright spots in the middle of micrograph. No presence of any void was detected in the "fine area".

The micrograph taken with higher resolution (Fig. 8b) demonstrates that voids were formed at the surface of the ODS particles and grow rather towards of the particles and not towards the matrix. This statement is confirmed by the analytical mapping which clearly shows that the formation of voids occurs inside the particles (Fig. 9b). The voids are visible with dark contrast in HAADF image (a) and in the Y map as spots with deficiency of yttrium (b).

### *3.2.3 450°C specimen*

The TEM characterization of material irradiated at 450°C shows the formation of dislocation loops with varying sizes from 30nm up to 100nm which were detected exclusively in the "coarse areas" (Fig. 10). Practically no loops with smaller sizes and no voids could be detected neither in the "coarse" nor in the "fine" areas. The loops imaged in Fig. 10 show correct oval projections on the image plane. Some large loops with d>50nm are not closed since they are cut by the foil surface. As their number density is almost negligible compared to irradiations at 350°C and below, no irradiation hardening has been detected [14] at 450°C irradiation temperature.

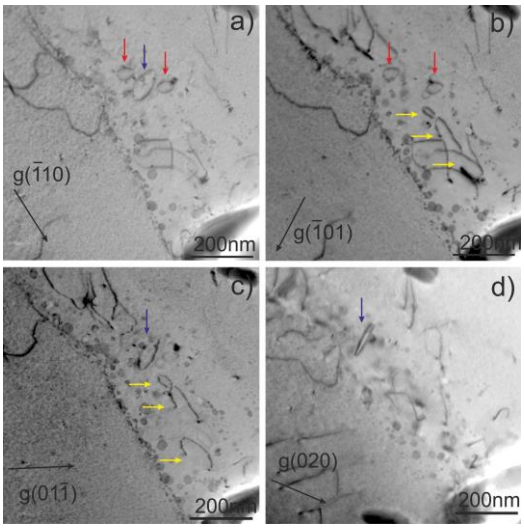


Fig. 10. The three images in the parts (a-c) were obtained from material irradiated at 450°C near [111] zone axis. The corresponding g-vectors are marked in the images. The image with [002] g vector (d) was obtained closely to the [102] zone axis.

Investigations using diffraction imaging show that all these large loops have Burgers vectors of [100] type. They all are visible in two of three <110> **g**-images near [111] zone axis (Fig. 10a-c). Since imaging near [111] zone axis does not allow a clear determination of the Burgers vector the specimen was tilted to [102] zone axis and imaged with $\boldsymbol{g}$=[020] ( Fig. 10d). The visibility criteria near the [111] zone axis and for $\boldsymbol{g}$=[010] are shown in Tab. 2. The loops

having [100] and [010] Burgers vectors are invisible in ***g***=[020] image. The single visible loop in the ***g***=[020] image has a [010] Burgers vector (Fig. 10d). The loops with corresponding Burgers vectors are marked by arrows with different colors.

| ***g*** \ ***b*** | ½[111] | ½[$\bar{1}$11] | ½[1$\bar{1}$1] | ½[11$\bar{1}$] | [001] | [010] | [100] |
|---|---|---|---|---|---|---|---|
| [$\bar{1}$10] | 0 | 1 | 0 | 0 | 0 | 1 | 1 |
| [$\bar{1}$01] | 0 | 1 | 1 | 1 | 1 | 0 | 1 |
| [01$\bar{1}$] | 0 | 0 | 1 | 1 | 1 | 1 | 0 |
| [020] | 1 | 1 | 1 | 1 | 0 | 2 | 0 |

Table. 2 |b·g| values for [111] beam direction and for ***g***=[020] near [102] zone axis.

The habit plane of the loops was determined by specimen tilting around the α or β axis. The loop marked with a blue arrow with ***b***=[010]{010} (blue arrow) shows inside contrast in the ***g***=[0$\bar{1}$1] image and outside contrast in the ***g***=[01$\bar{1}$] image. The loops with ***b***=[100]{100} show reversed contrast behaviors. The application of this method shows that all dislocation loops in this specimen have interstitial character (Fig. 11).

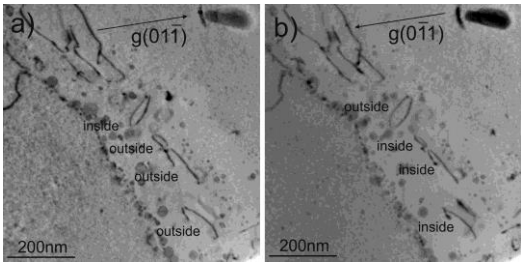


Fig. 11 g –g analysis which demonstrate whether dislocation loops have interstitial or vacancy character in the specimen irradiated at 450°C.

## 4. **Discussion:**

There are only few published result on microstructure of neutron irradiated ODS alloys. The stability of ODS particles under neutron irradiation and minor formation of dislocation structure was reported for radiation temperatures higher than 400°C [10]. The formation of small point defects, "black dots" was observed in neutron irradiated EUROFER-ODS alloy up to 3dpa dose at 300°C, 450°C and 550°C [11]. So far, 300°C is the lowest irradiation temperature for ODS steels reported in scientific literature. Such limited amount of published data and unequal irradiation conditions make a direct comparison of our own results with scientific literature less meaningful.

Our investigations clearly show the effect of ODS particles on the formation of radiation induced defects in EUROFER ODS alloy at all three irradiation temperatures. The radiation

induced black dots or small loops were observed in the specimen irradiated at 250°C exclusively in the "coarse area" (Fig. 3). Their number density is approximately one order of magnitude lower than the number density of defects formed in EUROFER 97 at the same conditions [22]. No radiation defects were observed in the fine area.

The material irradiated at 350°C shows a most complex radiation induced structure, which includes formation of both, dislocation loops and voids (Fig. 4-6). The TEM analysis of the dislocation loops showed them to be of interstitial character with both, <100> and ½<111> Burgers vectors. Loops of <100> type show a narrow size distribution with an average size of 15 nm while <111> loops have sizes up to 60 nm with an average of 27 nm. The number density of dislocation loops in the coarse area is also 3 times higher than in the fine area.

The ODS particles were found to be completely amorphous at all three irradiation temperatures. This was shown by application of both the HRTEM imaging and the results of convergent beam diffraction patterns. A higher magnification view of the voids is provided in Figure 8b. The voids where observed exclusively at ODS particles in the coarse area. It can be estimated that only a 30% fraction of the ODS particles in the coarse areas has attached voids.

In material irradiated at 450°C interstitial dislocation loops of <100> type with a size larger than 30 nm were found only in the coarse area (Fig. 10,11). The fine area was found to be free of any radiation induced defects. As the number density of these large loops is almost negligible compared to irradiations at 350°C and below, no irradiation hardening has been detected at 450°C irradiation temperature [14]. In contrast to our results the formation of small dislocation loops in neutron irradiated at 450°C ODS specimens was reported in ref. [11]. However, the Burgers vector analysis of these radiation induced defects was not performed.

The presented results show that formation radiation induced defects in ODS steels strongly depends on the density and distribution of ODS particles. The differences in defects formation between "coarse" and "fine" were observed for all irradiation temperatures. It can be concluded that ODS particles serve as defects sinks so that void formation takes place only at ODS particles with sizes larger than 5nm. Missing of voids and 3 times lower density of dislocation loops in "fine area" indicates that nanoparticles with high number density serve more effectively for radiation resistance than larger >10nm ODS particles with low number density. It can be also assumed that a "fine" distribution of ODS particles with 20 nm average inter-particle distance results in a significant reduction of further formation of structural defect compare to the ODS materials with average inter-particle size of 50-80nm, as in the coarse area or in PM2000 alloys.

Numerous ODS alloys were developed and fabricated during past decade. The number density of ODS particles varied from $10^{23}$ $m^{-3}$ in nanostructured ferritic alloys [19] down to $10^{22}$ $m^{-3}$ in ODS alloys of PM 2000 type [23]. The results presented here suggest that ODS alloys with a higher number density of fine nanoclusters should exhibit a higher radiation resistance than alloys with "coarse" ODS particles and low number density. The formation of dislocation loops and voids was observed only in the fine area only at 350°C. It should be mentioned that an irradiation temperature near 350°C is characterized by an increased (compared to higher >400°C or lower <300°C irradiation temperatures) production of radiation induced defects [24]. Different materials irradiated at 350°C demonstrate higher swelling due to the formation of cavities and a higher number density of dislocation loops [24,25]. The increased formation of voids at 350°C was also confirmed in pure and in boron alloyed EUROFER 97 irradiated at the same conditions [22,25]. The dislocation loops of both [100] and ½[111] types observed in specimens irradiated at 350°C and 450° show an interstitial character. This is a typical result for dislocation loops observed for different alloys [26].

The observation that irradiation induced hardening is more and more suppressed with increasing number density of oxide particles is obviously a common feature of ferritic-martensitic 9-10Cr ODS steels (like EUROFER-ODS) and nanoscaled ferritic 13-17Cr ODS steels (like 14YWT, [27,28]). Although this important observation is not yet quantitatively analyzed e.g. by computational materials science in the present literature, it seems now qualitatively obvious that (additional) irradiation induced loops will form only unlikely, if the existing sink strength density is already high enough. Or in other words, if in case of ODS steels the number density of nanoscaled ODS particles (e.g. $Y_2O_3$, $Y_2Ti_2O_5$) exceeds clearly the loop density of conventional ODS-particle-free casted steel irradiated under the same conditions. The critical number density is for 250-300°C neutron irradiations around $10^{22}$ $m^{-3}$. Above that ODS particle density, irradiation induced Frenkel defects will with a high probability not contribute to nucleation and growth of stable loops, but rather will annihilate by trapping at the ODS-particle matrix interface. Homogeneously dispersed, nanoscaled ODS particles have therefore an outstanding additional function: They are not only the cornerstone for high temperature creep and fatigue strength but also reduce remarkably irradiation hardening and consequently retard substantially irradiation embrittlement at least at tensile and creep relevant lower strain rates.

## 5. Conclusions:

The microstructure of neutron irradiated EUROFER–ODS material was characterized by TEM with application of WBDF imaging using different **g** vectors to study temperature dependent formation of radiation induced defects. The microstructural response as on neutron irradiation was found to be depend on the size and density of ODS particles. Reviewing all experimental results, the conclusion can be drawn that ODS materials have a higher radiation resistance than equivalent alloys without ODS particles. Moreover, the ODS materials with nanoclusters and high number density show a higher radiation resistance (lower defects density) at all temperatures than materials with low number density of ODS particles. The ODS particles were found to be in an amorphous state after irradiation at all three temperatures. The influence of neutron irradiation on size and number density of ODS particles cannot be determined.

The experimental results of quantitative characterization radiation induced defects at 250°C, 350°C and 450°C can be summarized as following:

-250°C irradiation temperature: Formation of "black dots" only in "coarse" area. Line dislocations show 3-4 times higher density in the coarse than in the fine area.

-350°C irradiation temperature: Formation of dislocation loops with sizes up to 60nm and ½<111> and <100> Burgers vectors in the "coarse" and in the "fine" areas. The number density of dislocation loops in the "coarse" area is 3 times than in the "fine" area. The loops show interstitial character.

-450°C irradiation temperature: Presence of interstitial loops with ½<111> Burgers vector and the size of 20-100nm in the "coarse" area.

At 250°C ODS particles strongly suppress the formation of displacement damage clusters, while in the specimens irradiated at 350°C both dislocation loops and cavities at the surface of ODS particles are observed, while at 450°C irradiation temperature large dislocation loops with sizes >30nm were detected.

**Acknowledgements:**

This work has been carried out within the framework of the EUROfusion Consortium and has received funding from the Euratom research and training programmme 2014-2018 under grant agreement No 633053. The views and opinions expressed herein do not necessarily reflect those of the European Commission.

References*:*


[1] J. Knaster, A. Moeslang, T. Muroga, Materials research for fusion, Nat. Phys. 5 (2016) 424–434. doi:10.1038/nphys3735.

[2] K. Ehrlich, The development of structural materials for fusion reactors, Philos. Trans. R. Soc. A Math. Phys. Eng. Sci. 357 (1999) 595–623. doi:10.1098/rsta.1999.0343.

[3] H.Z. M. Rieth, M. Schirra, A. Falkenstein, P. Graf, S. Heger, H. Kempe, R. Lindau, Eurofer 97 Tensile, Charpy, Creep and Structural Tests, (2003) 89. doi:0947-8620.

[4] E. Materna-Morris, A. Möslang, R. Rolli, H.C. Schneider, Effect of helium on tensile properties and microstructure in 9%Cr-WVTa-steel after neutron irradiation up to 15 dpa between 250 and 450 ??C, J. Nucl. Mater. 386–388 (2009) 422–425. doi:10.1016/j.jnucmat.2008.12.157.

[5] A. Möslang, C. Adelhelm, R. Heidinger, Innovative materials for energy technology, Int. J. Mater. Res. 99 (2008) 1045–1054. doi:10.3139/146.101743.

[6] A.A.F. Tavassoli, E. Diegele, R. Lindau, N. Luzginova, H. Tanigawa, Current status and recent research achievements in ferritic/martensitic steels, J. Nucl. Mater. 455 (2014) 269–276. doi:10.1016/j.jnucmat.2014.06.017.

[7] S. Chen, Y. Wang, K. Tadaki, N. Hashimoto, S. Ohnuki, Suppression effect of nano-sized oxide particles on helium irradiation hardening in F82H-ODS steel, J. Nucl. Mater. 455 (2014) 301–305. doi:10.1016/j.jnucmat.2014.06.041.

[8] C. Heintze, F. Bergner, M. Hernández-Mayoral, R. Kögler, G. Müller, A. Ulbricht, Irradiation hardening of Fe-9Cr-based alloys and ODS Eurofer: Effect of helium implantation and iron-ion irradiation at 300 °c including sequence effects, J. Nucl. Mater. 470 (2016) 258–267. doi:10.1016/j.jnucmat.2015.12.041.

[9] B. Yao, D.J. Edwards, R.J. Kurtz, TEM characterization of dislocation loops in irradiated bcc Fe-based steels, J. Nucl. Mater. 434 (2013) 402–410. doi:10.1016/j.jnucmat.2012.12.002.

[10] N. Akasaka, S. Yamashita, T. Yoshitake, S. Ukai, A. Kimura, Microstructural changes of neutron irradiated ODS ferritic and martensitic steels, J. Nucl. Mater. 329–333 (2004) 1053–1056. doi:10.1016/j.jnucmat.2004.04.133.

[11] M. Kolluri, P.D. Edmondson, N. V. Luzginova, F.A.V.D. Berg, A structure-property correlation study of neutron irradiation induced damage in EU batch of ODS Eurofer97

steel, Mater. Sci. Eng. A. 597 (2014) 111–116. doi:10.1016/j.msea.2013.12.074.

[12] A.I. Ryazanov, O.K. Chugunov, S.M. Ivanov, S.T. Latushkin, R. Lindau, A. Möslang, A.A. Nikitina, K.E. Prikhodko, E. V. Semenov, V.N. Unezhev, P. V. Vladimirov, Tensile properties and microstructure of helium implanted EUROFER ODS, J. Nucl. Mater. 442 (2013) S153–S157. doi:10.1016/j.jnucmat.2013.03.080.

[13] R. Lindau, A. Möslang, R.-D. Penzhorn, Mechanical and microstructural properties of tritium permeable PdAg alloy after helium implantation, J. Nucl. Mater. 191–194 (1992) 178–182. doi:10.1016/S0022-3115(09)80028-7.

[14] E. Materna-Morris, R. Lindau, H.C. Schneider, A. Möslang, Tensile behavior of EUROFER ODS steel after neutron irradiation up to 16.3 dpa between 250 and 450 °c, Fusion Eng. Des. 98–99 (2015) 2038–2041. doi:10.1016/j.fusengdes.2015.07.015.

[15] N. Baluc, R. Schäublin, P. Spätig, M. Victoria, On the potentiality of using ferritic/martensitic steels as structural materials for fusion reactors, Nucl. Fusion. 44 (2003) 56–61. doi:10.1088/0029-5515/44/1/006.

[16] E. Materna-Morris, A. Möslang, H. Schneider, Tensile and low cycle fatigue properties of EUROFER97-steel after 16 . 3 dpa neutron irradiation at 523 , 623 and 723 K, J. Nucl. Mater. 442 (2013) S62–S66. doi:10.1016/j.jnucmat.2013.03.038.

[17] R. Lindau, M. Klimenkov, U. Jäntsch, A. Möslang, L. Commin, Mechanical and microstructural characterization of electron beam welded reduced activation oxide dispersion strengthened - Eurofer steel, J. Nucl. Mater. 416 (2011) 22–29. doi:10.1016/j.jnucmat.2011.01.025.

[18] R. Schaeublin, T. Leguey, P. Spätig, N. Baluc, M. Victoria, Microstructure and mechanical properties of two ODS ferritic/martensitic steels, J. Nucl. Mater. 307–311 (2002) 778–782. doi:10.1016/S0022-3115(02)01193-5.

[19] G.R. Odette, Recent Progress in Developing and Qualifying Nanostructured Ferritic Alloys for Advanced Fission and Fusion Applications, Jom. 66 (2014) 2427–2441. doi:10.1007/s11837-014-1207-5.

[20] C.C. Eiselt, M. Klimenkov, R. Lindau, A. Möslang, H.R.Z. Sandim, A.F. Padilha, D. Raabe, High-resolution transmission electron microscopy and electron backscatter diffraction in nanoscaled ferritic and ferritic-martensitic oxide dispersion strengthened-steels, J. Nucl. Mater. 385 (2009) 231–235. doi:10.1016/j.jnucmat.2008.11.029.

[21] P. He, M. Klimenkov, R. Lindau, A. Möslang, Characterization of precipitates in nano structured 14% Cr ODS alloys for fusion application, J. Nucl. Mater. 428 (2012) 131–138. doi:10.1016/j.jnucmat.2011.08.026.

[22] M. Klimenkov, E. Materna-Morris, A. Möslang, Characterization of radiation induced defects in EUROFER 97 after neutron irradiation, J. Nucl. Mater. 417 (2011) 124–126. doi:10.1016/j.jnucmat.2010.12.261.

[23] M. Klimiankou, R. Lindau, A. Möslang, J. Schröder, TEM study of PM 2000 steel, Powder Metall. 48 (2005) 277–287. doi:10.1179/174329005X64171.

[24] A. Kimura, T. Morimura, M. Narui, H. Matsui, Irradiation hardening of reduced activation martensitic steels, J. Nucl. Mater. 233–237 (1996) 319–325. doi:10.1016/S0022-3115(96)00233-4.

[25] M. Klimenkov, A. Möslang, E. Materna-Morris, H.C. Schneider, Helium bubble morphology of boron alloyed EUROFER97 after neutron irradiation, J. Nucl. Mater. 442 (2013) S52–S57. doi:10.1016/j.jnucmat.2013.04.022.

[26] A. Kimura, Current Status of Reduced-Activation Ferritic/Martensitic Steels R&D for Fusion Energy, Mater. Trans. 46 (2005) 394–404. doi:10.2320/matertrans.46.394.

[27] D.A. McClintock, M.A. Sokolov, D.T. Hoelzer, R.K. Nanstad, Mechanical properties of irradiated ODS-EUROFER and nanocluster strengthened 14YWT, J. Nucl. Mater. 392 (2009) 353–359. doi:10.1016/j.jnucmat.2009.03.024.

[28] S.J. Zinkle, A. Möslang, T. Muroga, H. Tanigawa, Multimodal options for materials research to advance the basis for fusion energy in the ITER era, Nucl. Fusion. 53 (2013) 104024. doi:10.1088/0029-5515/53/10/104024.